Application of Quasi-Heat-Pulse Solutions for Luikov's Equations of Heat and Moisture Transfer for Calibrating and Utilizing Thermal Properties Apparatus[1]

Mark A. Dietenberger and Charles R. Boardman
USDA Forest Service, Forest Products Laboratory
One Gifford Pinchot Drive, Madison Wisconsin 53726-2398
mdietenberger@fs.fed.us, cboardman@fs.fed.us

ABSTRACT

Several years ago the Laplace transform solutions of Luikov's differential equations were presented for one-dimensional heat and moisture transfer in porous hydroscopic orthotropic materials for the boundary condition of a gradual heat pulse applied to both surfaces of a flat slab. This paper presents calibration methods and data for the K-tester 637 (Lasercomp), allowing use of the mathematical solutions to measure material properties. The K-tester supplies a quasi-heat-pulse to both sides of a 2-ft-square specimen and records signals as function of time from surface thermocouples and thermopiles. Analysis methods are presented that apply to the thermal wave traveling through the FR4 thermopile, copper cladding, a sheet facing (aluminum or particle board), and the test specimen. A heavier, thicker, and expanded polystyrene (PS) foam board traceable to NIST was used as a "standard" specimen for calibrating thermal properties and temperature differential (from thermopile microvolts) for the FR4 thermopile via a specialized "forked" heat pulse profile. The similar heat pulse profile was then used to determine heat capacities and thermal conductivities of a very heavy and pure polystyrene board, Rexolite 1422, and a very light and thinner extruded PS foam board, in basic agreement with independent measurements. In addition, formulae are obtained for heat capacities and thermal conductivities of PS-based boards as functions of density, structure, and temperature. The stage is set for future work for determining heat and moisture transfer properties for a moist wood core between aluminum plate facings.

Keywords: Luikov equations solutions, heat/moisture transfer properties, foam core boards

INTRODUCTION

A practical test method for thermal property testing of many building materials must be limited to high-aspect-ratio flat slab geometry, particularly for orthotropic wood material, which eliminates many short-pulse heat methods provided in the literature [1-3]. Sandwich boards such as foam core particleboards made in a one-step manufacturing process will require high-aspect flat slab geometry for thermal properties testing. Methods using sustained heat pulse or steady-state conditions [4, 5] are subject to strong moisture migration effects within hygroscopic materials, which can lead to inconsistencies in the derived conductive heat transfer properties. Methods developed for soft organic matter, which involve measuring moisture and temperature profiles within the specimen, are difficult to apply to wood-based materials. More comprehensive heat and moisture transfer solutions are therefore needed for property evaluations.

To address these limitations, the analytical Laplace transform solution to the Luikov's differential equations for one-dimensional heat and moisture transfer [6-10] and for a gradual finite heat pulse applied to both surfaces of a flat panel is implemented in a recursive time discretization formulation for use in an Excel spreadsheet. The transient heat and moisture

[1] This paper was prepared by U.S. Government employees on official time and is therefore in the public domain and not subject to copyright in the United States.

transfer solution is general enough to accommodate a multilayer composite. To be most useful in deriving the properties, the composite panel is optimally constructed of a thick core material (foam or wood) that serves as a specimen while the relatively thin facing densified layers between the heat pulse load and the specimen assist in conditioning the specimen boundary conditions and maintaining a one-dimensional heat and moisture flow through the panel. The moist, porous, temperature-dependent, and orthotropic material under constant pressure has the coupled transient partial differential heat and mass transfer expressed as

$$\rho C_q \frac{\partial T}{\partial t} = \nabla \bullet \left(K_q \bullet \nabla T\right) + \varepsilon \lambda \rho C_m \frac{\partial U}{\partial t} \tag{1}$$

$$\rho C_m \frac{\partial U}{\partial t} = \nabla \bullet \left(K_m \bullet \left[\nabla U + \delta \nabla T\right]\right) \tag{2}$$

where T is temperature (K), U is moisture potential (MCg), t is time (s), K_q and K_m are thermal and moisture conductivity coefficients (kW/mK, g/smK), C_q and C_m are heat and moisture capacities (kJ/gK, MCg/gK), ρ is dry body density (kg/m^3), ε is ratio of vapor diffusion coefficient to coefficient of total moisture diffusion, λ is heat of phase change (kJ/g), and δ is the thermogradient coefficient (MCg/K).

The simplest analysis is to apply a steady heat flux, but zero mass flux, across the boundaries in a principal direction of the material. This zeroes the term $\nabla U + \delta \nabla T$ in that principal direction and thus defines the moisture migration condition at steady state. Consequently one obtains a constant heat flux $\vec{q}'' = K_q \bullet \nabla T$ across the principal direction. Using a steady-state apparatus for high-aspect-ratio samples remains complicated because the thermal conductivity and mass conductivity [6] generally increase with both temperature T and moisture content $C = C_m U$. The result is a nonlinear distribution of both temperature and moisture content across the sample thickness. A second simple analysis is to apply a constant mass flux, but zero heat flux, across the boundaries in a principal direction of the material. By measuring both temperature and moisture profiles within the sample in this test procedure, the value of mass conductivity K_m can also be derived as function of temperature and moisture content. The heat capacity C_q and heat of phase change λ can be obtained from differential scanning calorimeter measurements. This two-step procedure was used for evaluating certain food materials, such as bread [11]. For wood, there is the difficulty of obtaining reliable simultaneous temperature and moisture profiles within the specimen.

A third simplified analysis is to consider that the mass diffusivity is two orders of magnitude less than thermal diffusivity. This approach utilizes specialized transient methods [6]; that is, to obtain moisture conductivity K_m, the sample would be subjected to a sustained change in moisture loss rate while keeping its temperature at a steady value, as approximately in a high-velocity, very dry convective environment. Whereas, for obtaining the thermal properties C_q and $K_{eff} = K_q + \varepsilon \lambda \delta \, K_m$, a short heat conductive pulse instead would be applied to the sample in a way that allows the thermal wave to dissipate fairly rapidly before significant changes occur in the moisture profile. Thus while the specimen gradually reaches some uniform temperature, any slight perturbation in the moisture profile due to short heat-pulse-generated water flux $\vec{m}''_q = \delta K_m \bullet \nabla T$ is gradually flattened back to the original uniform moisture profile. This moisture movement also involves the latent heat of water, which significantly perturbs the conductive heat transfer process. This quasi-heat-pulse method preserves the average moisture content of the wood slab and prevents severe gradients from occurring along the slab so as to preserve one-dimensional flow processes

across the slab. If the perturbing moisture profile is also too great, then the coupled Equations (1) and (2) need to be solved, for which only a few analytical solutions are available in the literature. Analytical solutions for three relevant boundary conditions with time discretization are provided in an earlier paper [12] and are summarized in the solution section. The series solution is reformulated into a recursive form for easy and efficient implementation on a computer. For the current specimen, this implementation occurs in two stages. The first stage is to use a standard reference PS foam board with known heat capacity and thermal conductivity to calibrate for the temperature differentials from the coefficients relating to the microvolts signals for the K-tester thermopile and to calibrate the thermopile's heat capacity and thermal conductivity. The second stage is the specimen testing of Rexolite 1422 pure PS and extruded low-density PS foam boards to determine their heat capacity and thermal conductivity using the calibrated parameters associated with the thermopile.

TIME DISCRETIZATION THERMAL/MOISTURE SOLUTION FOR EACH MATERIAL LAYER

The boundary conditions to solve Equations (1) and (2) require that just four conditions be given on either or both interface surfaces, of which three relevant forms (of a possible 70 forms) are provided here. For the center core material, the boundary conditions (BC) are the heat and moisture fluxes on both surfaces (as interfaces within the K-tester) of the material as a function of time solved for temperature and moisture content profile with time. For the interface layers of copper, aluminum, or particleboard, the BC is the heat and moisture flux on the heat pulse side as well as the associated surface temperature and moisture. Obviously, moisture content is zero for solid metals and dried particleboard. The transient temperature and moisture content profiles are then solved for the interface slab, and heat and moisture surface fluxes on the opposing side of the heat pulse side are calculated as well. For the thermopile, the BC is the surface temperature and moisture content on both interfaces of the thermopile as function of time. The resulting solution is the transient temperature and moisture profile and surface heat and moisture fluxes at the interfaces. Here again, moisture content is zero for the existing thermopile. For some future study one might introduce the concept of a permeable thermo-moist-pile for use on a hygroscopic wall, such as cross-laminated timber, to take full advantage of the solutions provided here.

Time-discretization Solution for the Core Material

By representing boundary conditions as approximately stepping functions, the time discretization form of the solution [12] to Equations (1) and (2) for the core material is

$$
\begin{aligned}
&(1-\delta\delta^*)(a-b)\begin{Bmatrix} T(\hat{x},t) \\ U(\hat{x},t) \end{Bmatrix} \cong \\
&\sum_{i=0}^{n} \begin{Bmatrix} a-1/\alpha_m \\ -a\delta \end{Bmatrix} \left[\frac{\Delta\dot{q}''(\ell,t_i)}{K_{q,\ell}+\varepsilon\lambda K_{m,\ell}\delta} S(a,\hat{x},t-t_i) - \frac{\Delta\dot{q}''(0,t_i)}{K_{q,0}+\varepsilon\lambda K_{m,0}\delta} S(a,\ell-\hat{x},t-t_i) \right] \\
&+\sum_{i=0}^{n} \begin{Bmatrix} 1/\alpha_m-b \\ b\delta \end{Bmatrix} \left[\frac{\Delta\dot{q}''(\ell,t_i)}{K_{q,\ell}+\varepsilon\lambda K_{m,\ell}\delta} S(b,\hat{x},t-t_i) - \frac{\Delta\dot{q}''(0,t_i)}{K_{q,0}+\varepsilon\lambda K_{m,0}\delta} S(b,\ell-\hat{x},t-t_i) \right] \\
&+\sum_{i=0}^{n} \begin{Bmatrix} -a\delta^* \\ a-1/\alpha^* \end{Bmatrix} \left[\frac{\Delta\dot{m}''(\ell,t_i)}{K_{m,\ell}} S(a,\hat{x},t-t_i) - \frac{\Delta\dot{m}''(0,t_i)}{K_{m,0}} S(a,\ell-\hat{x},t-t_i) \right] \\
&+\sum_{i=0}^{n} \begin{Bmatrix} b\delta^* \\ 1/\alpha^*-b \end{Bmatrix} \left[\frac{\Delta\dot{m}''(\ell,t_i)}{K_{m,\ell}} S(b,\hat{x},t-t_i) - \frac{\Delta\dot{m}''(0,t_i)}{K_{m,0}} S(b,\ell-\hat{x},t-t_i) \right]
\end{aligned}
\tag{3}
$$

where various terms in this equation are defined as follows:

$$\alpha^* = \frac{K_q + \varepsilon\lambda K_m \delta}{\rho C_q} = \alpha_q + \frac{\varepsilon\lambda K_m \delta}{\rho C_q} \quad (4)$$

$$\delta^* = \frac{\varepsilon\lambda K_m}{K_q + \varepsilon\lambda K_m \delta} \quad (5)$$

$$\alpha_m = \frac{K_m}{\rho C_m} \quad (6)$$

$$a = \frac{\alpha_m + \alpha^*}{2\alpha_m\alpha_q} + \sqrt{\left(\frac{\alpha_m + \alpha^*}{2\alpha_m\alpha_q}\right)^2 - \frac{1}{\alpha_m\alpha_q}}$$

$$b = \frac{\alpha_m + \alpha^*}{2\alpha_m\alpha_q} - \sqrt{\left(\frac{\alpha_m + \alpha^*}{2\alpha_m\alpha_q}\right)^2 - \frac{1}{\alpha_m\alpha_q}} \quad (7)$$

$$S(a,\hat{x},t) = \frac{t}{a\ell} + \ell\left\{\frac{3\hat{x}^2 - \ell^2}{6\ell^2} - \frac{2}{\pi^2}\sum_{n=1}^{\infty}\frac{(-1)^n}{n^2}\exp\left[\frac{-t}{a}\left(\frac{n\pi}{\ell}\right)^2\right]\cos\left(\frac{n\pi\hat{x}}{\ell}\right)\right\} \quad (8)$$

In Equation (8), the term *a* is substituted with the term *b* where it is needed in Equation (3). Intuitively, this time discretization solution is just a series of innumerous micro-thermal/moisture-waves into the material. Close examination of the response function in Equation (8) suggests a generic conversion to a fully recursive form as follows:

$$\begin{aligned} I_{f,m} &\equiv \sum_{i=0}^{m}\Delta f(t_i)\left(\frac{t_{m+1} - t_i}{a\ell} + \ell\frac{3\hat{x}^2 - \ell^2}{6\ell^2}\right) \\ &= I_{f,m-1} + \left(f(t_{m+1/2}) - f(t_{0-1/2})\right)\left(\frac{t_{m+1} - t_m}{a\ell}\right) + \Delta f(t_m)\left(\ell\frac{3\hat{x}^2 - \ell^2}{6\ell^2}\right) \end{aligned} \quad (9)$$

$$\begin{aligned} J_{f,n,m} &= \sum_{i=0}^{i=m}\Delta f(t_i)\exp\left[\frac{-(t_{m+1} - t_i)}{a}\left(\frac{n\pi}{\ell}\right)^2\right] \\ &= \left(J_{f,n,m-1} + \Delta f(t_m)\right)\exp\left[\frac{-(t_{m+1} - t_m)}{a}\left(\frac{n\pi}{\ell}\right)^2\right] \end{aligned} \quad (10)$$

A dramatic reduction in memory and computation requirements occurs. The method provides for variable time steps, as typically happens in the K-tester. The first eight terms in the series of Equation (5) are sufficient for a three-digit precision. The intriguing aspect of the discretized solution above is the coupled explicit solutions of heat and moisture transfer, with their two-order-of-magnitude differences in the time scale of their physical processes. Contrasting with this are the finite difference methods that require specialized matrix equation solvers or additional constructs of elaborate spatial discretization to overcome the time-scale differences between heat and moisture transport.

Time-discretization Solution for the Interfacing Materials

The Duhamel analytical solution for the interfacing material as shown in [12] is not presented in the time discretization form. This paper now reports it in the time discretization form as

$$
\begin{aligned}
T(\hat{x},t) &= \sum_{i=0}^{n} \Delta T(0,t_i)\left(\frac{ab\alpha_m - b}{a-b}P(a,\hat{x},t-t_i) + \frac{a-ab\alpha_m}{a-b}P(b,\hat{x},t-t_i)\right) \\
&+ \sum_{i=0}^{n}\left(\frac{\Delta\dot{q}''(0,t_i)}{(1-\delta\delta^*)(K_q+\varepsilon\lambda K_m\delta)} - \frac{\delta^*\Delta\dot{m}''(0,t_i)}{(1-\delta\delta^*)(K_m)}\right)\left(\frac{ab\alpha_m - b}{a-b}Q(a,\hat{x},t-t_i) + \frac{a-ab\alpha_m}{a-b}Q(b,\hat{x},t-t_i)\right) \\
&+ \sum_{i=0}^{n}\Delta U(0,t_i)\left(\frac{\delta^* ab\alpha^*}{a-b}\left(-P(a,\hat{x},t-t_i)+P(b,\hat{x},t-t_i)\right)\right) \\
&+ \sum_{i=0}^{n}\left(\frac{\Delta\dot{m}''(0,t_i)}{(1-\delta\delta^*)(K_m)} - \frac{\delta\Delta\dot{q}''(0,t_i)}{(1-\delta\delta^*)(K_q+\varepsilon\lambda K_m\delta)}\right)\left(\frac{\delta^* ab\alpha^*}{a-b}\left(-Q(a,\hat{x},t-t_i)+Q(b,\hat{x},t-t_i)\right)\right) \\
U(\hat{x},t) &= \sum_{i=0}^{n}\Delta T(0,t_i)\left(\frac{\delta ab\alpha_m}{a-b}\left(-P(a,\hat{x},t-t_i)+P(b,\hat{x},t-t_i)\right)\right) \\
&+ \sum_{i=0}^{n}\left(\frac{\Delta\dot{q}''(0,t_i)}{(1-\delta\delta^*)(K_q+\varepsilon\lambda K_m\delta)} - \frac{\delta^*\Delta\dot{m}''(0,t_i)}{(1-\delta\delta^*)(K_m)}\right)\left(\frac{\delta ab\alpha_m}{a-b}\left(-Q(a,\hat{x},t-t_i)+Q(b,\hat{x},t-t_i)\right)\right) \\
&+ \sum_{i=0}^{n}\Delta U(0,t_i)\left(\frac{ab\alpha^* - b}{a-b}P(a,\hat{x},t-t_i) + \frac{a-ab\alpha^*}{a-b}P(b,\hat{x},t-t_i)\right) \\
&+ \sum_{i=0}^{n}\left(\frac{\Delta\dot{m}''(0,t_i)}{(1-\delta\delta^*)(K_m)} - \frac{\delta\Delta\dot{q}''(0,t_i)}{(1-\delta\delta^*)(K_q+\varepsilon\lambda K_m\delta)}\right)\left(\frac{ab\alpha^* - b}{a-b}Q(a,\hat{x},t-t_i) + \frac{a-ab\alpha^*}{a-b}Q(b,\hat{x},t-t_i)\right)
\end{aligned}
\tag{11}
$$

Where the terms for *P* and *Q* are defined as

$$
P(a,\hat{x},t) = 1 - \frac{4}{\pi}\sum_{n=0}^{\infty}\frac{1}{2n+1}\exp\left(\frac{-t}{a}\left[\frac{(2n+1)\pi}{2\ell}\right]^2\right)\sin\left(\frac{(2n+1)\pi\hat{x}}{2\ell}\right) \tag{12}
$$

$$
Q(a,\hat{x},t) = \hat{x} - \frac{8\ell}{\pi^2}\sum_{n=0}^{\infty}\frac{1}{(2n+1)^2}\exp\left(\frac{-t}{a}\left[\frac{(2n+1)\pi}{2\ell}\right]^2\right) * \left(1-\cos\left[\frac{(2n+1)\pi\hat{x}}{2\ell}\right]\right) \tag{13}
$$

The term *b* can be substituted for the term *a* when appropriate. The generic Equations (9) and (10) are used to convert Equation (11) into the recursive form for implementation in the Excel spreadsheet. We also note that the first derivative with respect to the *x* variable of Equation (11) as evaluated at the interface thickness and multiplied by the respective thermal and moisture conductivities provides the BC of heat and moisture fluxes for the next inner interface material, or to the final core material.

Time-discretization Solution for the Thermopile

The Duhamel analytical solution for the thermopile material as shown in [12] is not presented in the time discretization form. This paper now reports it in the time discretization form as

$$
\begin{aligned}
(a-b)\begin{Bmatrix} T(\hat{x},t) \\ U(\hat{x},t) \end{Bmatrix} &= \sum_{i=0}^{n} \begin{Bmatrix} ab\alpha_m - b \\ -\delta ab\alpha_m \end{Bmatrix} \left[\Delta T(\ell,t_i) R(a,\hat{x},t-t_i) + \Delta T(0,t_i) R(a,\ell-\hat{x},t-t_i)\right] \\
&+ \sum_{i=0}^{n} \begin{Bmatrix} a - ab\alpha_m \\ \delta ab\alpha_m \end{Bmatrix} \left[\Delta T(\ell,t_i) R(b,\hat{x},t-t_i) + \Delta T(0,t_i) R(b,\ell-\hat{x},t-t_i)\right] \\
&+ \sum_{i=0}^{n} \begin{Bmatrix} -\delta^* ab\alpha^* \\ ab\alpha^* - b \end{Bmatrix} \left[\Delta U(\ell,t_i) R(a,\hat{x},t-t_i) + \Delta U(0,t_i) R(a,\ell-\hat{x},t-t_i)\right] \\
&+ \sum_{i=0}^{n} \begin{Bmatrix} \delta^* ab\alpha^* \\ a - ab\alpha^* \end{Bmatrix} \left[\Delta U(\ell,t_i) R(b,\hat{x},t-t_i) + \Delta U(0,t_i) R(b,\ell-\hat{x},t-t_i)\right]
\end{aligned}
\qquad (14)
$$

Where the term *R* is evaluated with the equation,

$$
R(a,\hat{x},t) = \frac{\hat{x}}{\ell} + \frac{2}{\pi}\sum_{n=1}^{\infty} \frac{\cos(n\pi)}{n} \exp\left[\frac{-t}{a}\left(\frac{n\pi}{\ell}\right)^2\right] \sin\left(\frac{n\pi\hat{x}}{\ell}\right) \qquad (15)
$$

Once again the generic recursive Equations (9) and (10) are applied for implementation into the Excel spreadsheet. Corresponding to the BC of temperature and moisture content on both sides of this interface slab is the solution to the temperature and moisture profile as a function of time. By taking the derivative of Equation (14) with respect to *x* as evaluated at the interface surface and multiplied by the thermal and moisture conductivities, the heat and moisture fluxes on both interface surfaces are obtained. This in turn is used as BC for the previous solution to the interfacing materials. The moisture content is set to zero in the case of the thermopile.

THERMOPILE CALIBRATION USING REFERENCE PS MATERIALS

The pure polystyrene as obtained with the 25.4 mm thick Rexolite 1422 provided a uniform density of 1046 kg/m^3 to within a fraction of a percent, in contrast to the standard expanded polystyrene bulk density of 51 kg/m^3 that may have large local variations of 10% or more in the density [13]. From the National Institute of Standards and Technology (NIST) material databank on-line, the values and formula for heat capacities of optical graded pure polystyrene (SRM-705a) is given as

$$
C_{q,PS} = 1113.48 + 4.3849(T - 273.15) + 0.000857(T - 273.15)^2 \qquad \text{kJ/gK} \quad (16)
$$

Pieces of Rexolite cut from the four corners of the 600- by 600-mm specimen are measured for heat capacity in a differential scanning calorimeter (DSC). Indications are that heat capacity values of Rexolite are 6% less than that of SRM-705a on average, presumably due to the differences in the crystalline structure. The K-tester is also used with the Rexolite in the steady state mode to determine the thermal conductivities of 0.1598 W/mK at 25.14 ^{o}C and 0.1614 W/mK at 35.16 ^{o}C. This resulted in a reasonable function for thermal conductivity of Rexolite as a function of temperature,

$$
K_{q,PS} = 0.0289T^{0.3} \qquad \text{W/mK} \qquad (17)
$$

To make further progress, the thermopile will need to be calibrated differently when the K-tester is used in the transient mode using a quasi-heat pulse. There is a transient delay in the heat passing to the specimen, as when the heat is impulsively applied from the aluminum plate/rubber mat to the thermopile, in that the thermal wave must pass through the thermopile, the copper plating, an interface facing, and finally into the specimen. The thermocouple within the very thin copper plating is used for controlling the set points for temperature changes for upper and lower surfaces. If the upper and lower plates are set at the same small temperature increment (i.e., 10 °C as shown in Figure 1 for the standard foam material), then the total heat absorbed during the whole period of heating until steady state is achieved is given merely by the product of material heat capacity, material mass, and temperature rise as summed over all affected materials. The microvolt signals from the thermopiles are converted to temperature differential across the thermopiles via calibration constants that themselves have a small linear variation with temperature, and possibly some sensitivity with the time step chosen. The thermopile substrate is a thermoset laminate (FR4) with a thin copper cladding (their thicknesses were provided by Lasercomp company), so their nominal thermal properties of heat capacities, thermal conductivities, and densities are adopted from Eveloy and others [14], except that the thermopile heat capacity is allowed to be adjusted by a few percent and be calibrated during the curve fitting process.

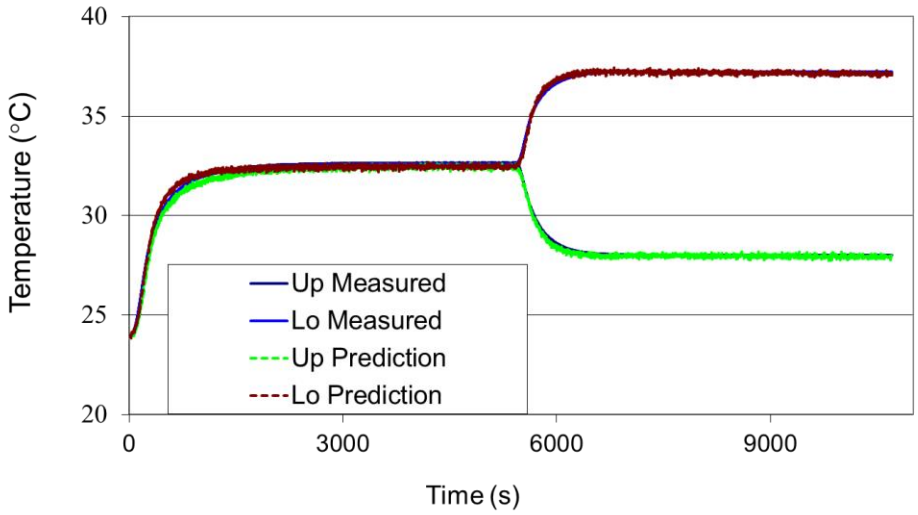

Fig. 1. Interface temperature predictions versus measurement with calibrated thermopile for standard expanded foam (Up = upper copper plate, Lo = lower copper plate)

Equation (14) for upper and lower thermopiles is used to calculate heat fluxes into the interface materials between the thermopiles and the specimen, thus accounting fully for the effects of thermal waves into the calibration process. Equation (11) for the interface materials is used to calculate delayed and reduced heat fluxes into both sides of the specimen as a result of interface material heat absorption and thermal wave effects. Equation (3) for the specimen provides the transient response, in which the surface temperatures (and surface moisture if the specimen has moisture flow) are calculated as a function of time and compared with the "measured" temperatures of both upper (Up) and lower (Lo) copper plates. This comparison should be very close, as in Figure 1, if the values for the heat capacity and thermal conductivity of the materials are correct and the thermopile coefficients are well calibrated.

To increase the role of the thermal conductivity Equation (17), another heat pulse after 2.5 hours is applied to the lower surface to increase it a further 5 °C, and a cooling pulse applied to the upper surface to decrease it by 5 °C. This is shown in Figure 1 for temperature response in the copper plates and in Figure 2 for the microvolt signals of the thermopile. The heating and cooling pulses will settle at constant levels, as shown in Figure 2, to maintain a constant temperature differential between the upper (Up) and lower (Lo) surfaces. Recall that Equation (14) and coefficients of thermopile microvolts are used to convert the thermopile signal into transient heat fluxes values for the specimen BC. During these changes, there is no net increase in the heat content of the specimen, thus removing the influence of heat capacity during the second pulse, except during the transient change in the interface temperatures. Because this is a second method to calibrate the thermopile coefficients that is based on a thermal conductivity reference value, Equations (16) and (17) must be compatible for close predictions for the whole profile that include the two pulse phases, which we labeled as the forked pulsing method.

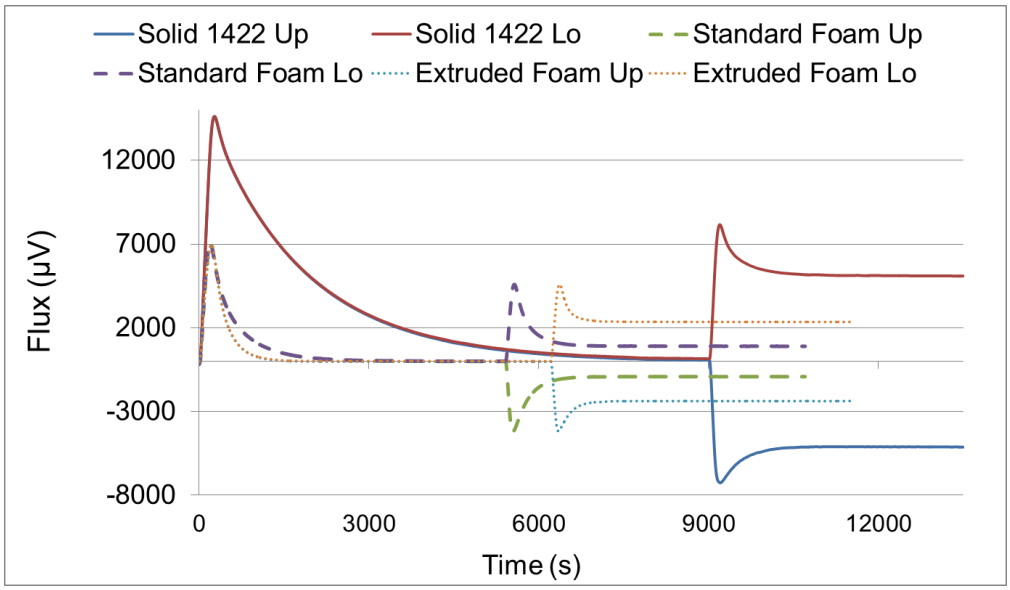

Fig. 2. Thermopile microvolt signals associated with temperature profiles in Fig. 3 for Rexolite PS board, Fig. 1 for standard expanded PS foam, and Fig. 4 for extruded PS foam

In consideration of the expanded polystyrene foam, the values for density, heat capacity and thermal conductivity for pure PS are extended to the solid PS portion of the foam material. In addition, the density, heat capacity, and thermal conductivity of air as functions of temperature are obtained from the NIST material databank on-line for use with the void fraction of the expanded polystyrene. The bulk heat capacity of the foam is then the mass weighted between the heat capacity of pure PS and heat capacity of air. The thermal conductivity is dependent on the cellular structure of the foam. If the cellular walls are totally parallel to the heat flow direction, then the foam thermal conductivity is a paralleled mass weighted between the pure PS and air. If the cellular walls at the opposite extreme are layered perpendicular with respect to the heat flow direction, the foam thermal conductivity would be series weighted between the pure PS and air. Included is also a radiative heat conductivity component pertaining to the void space of the foam [15], which can provide an added 9% of the extruded PS foam base value of thermal conductivity [12]. In reality the foam structure is somewhere between parallel and series layered, for which a fraction parameter is used. With the K-tester in the steady state mode at average temperature of 32.6 °C, the measured thermal conductivity for the standard foam board is 0.0353 W/mK, which corresponds to the fraction parameter set at 0.92. Comparisons at other temperatures show that three significant digits

accuracy is maintained with the fraction parameter remaining at 0.92. This indicated the dominance of the parallel structure of the expanded PS foam. In any case, with no adjustment needed to either Equation (16) or (17), we have obtained the results in Figure 1 with a fit to the data having the correlation coefficient of 0.998 for both upper and lower measurements with the contributions from both cells #2 and #3 of the K-tester.

The significance of the fork pulse method can be appreciated when it is considered that the situation is actually that of a foam core faced with the thermopile layers in the sensing region. That is, the Excel solver is set up to allow changes in the thermopile heat capacity and the foam solid matrix heat capacity to fit temperature profile, while at the same time optimizing the microvolt conversion to temperature differential to match the thermal conductivity correlation. An optimum ratio of heat capacities is needed to match the transient hill of the measured temperature profile for a low-density foam material.

REXOLITE 1422 BOARD - HEAT CAPACITY AND THERMAL CONDUCTIVITY CONFIRMATION

On the other hand, the high mass of the 25.4 mm thick Rexolite board reduces significantly the sensitivity of the time discretized solutions to the thermopile heat capacity, confirming the role of the expanded PS foam in calibrating any parameters associated with the thermopile. Therefore the calibrated values for thermopiles' microvolt conversion to temperature differentials, heat capacity, and thermal conductivity were extended from the expanded PS foam to the Rexolite 1422 material. Results shown in Figure 3 with the Rexolite specimen indicate that the heat capacity needs to be 1.7% less than that of heat capacity equation, Equation (16), and no adjustment needed to the thermal conductivity equation, Equation (17), from the curve fitting to the forked pulse temperature profile with a correlation coefficient of 0.998. The 1.7% reduction obtained in the heat capacity of amorphous Rexolite from that of optically pure PS at least goes in the same direction as the DSC results of 6% reduction. We also note that the thermopile microvolt signals for Rexolite (Figure 2) is much higher and longer duration than that of the expanded foam, indicating the linearity of the thermopile calibration over wide range of values for both heat capacity and thermal conductivity.

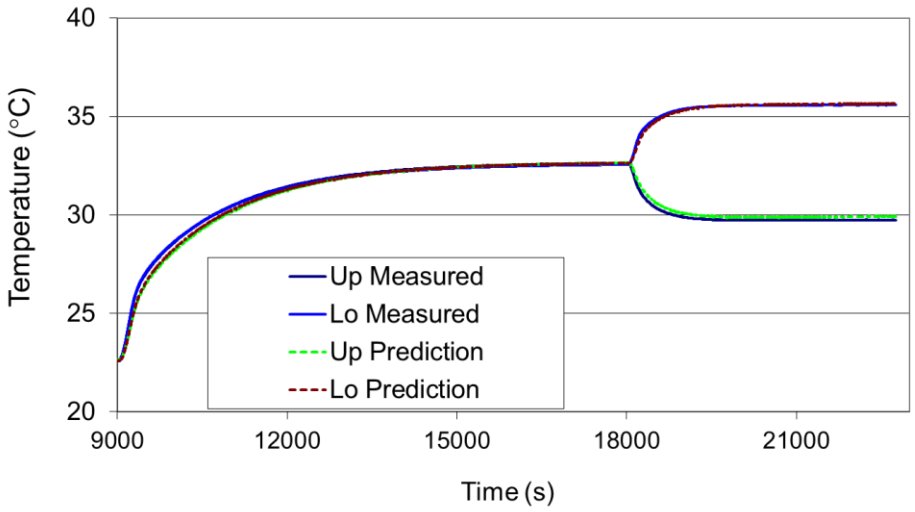

Fig. 3. Interface temperature predictions versus measurement with calibrated thermopile for Rexolite 1422 PS board (Up = upper copper plate, Lo = lower copper plate)

EXTRUDED PS FOAM — HEAT CAPACITY AND THERMAL CONDUCTIVITY EVALUATION

The fork heat pulsing technique is then applied to the 14.9-mm-thick extruded PS foam at density of 25.7 kg/m^3 to test the calibration and predictability at the other extreme for a very light board that is also relatively thin. The predictions versus measured temperature of the fork pulsed heating (Figure 4) shows agreement with a correlation coefficient of 0.998. Because of the extreme sensitivity at low heat loading, raw data from two of the cells are combined linearly to allow the heat fluxes calculated with the thermopile in the transient mode to provide a flat temperature prediction at steady state. This combining of data is also applied to the expanded foam and Rexolite with equally good results. When the extruded foam is tested in the K-tester at equilibrium conditions, the thermal conductivity values are such that the fraction parameter could be set at 0.52 to a three significant value accuracy, which is also found suitable for the transient mode. Again, no further adjustment is needed to the heat capacity formula (16) as used in a mass weighted form with the air heat capacity in order to obtain the results in Figure 4.

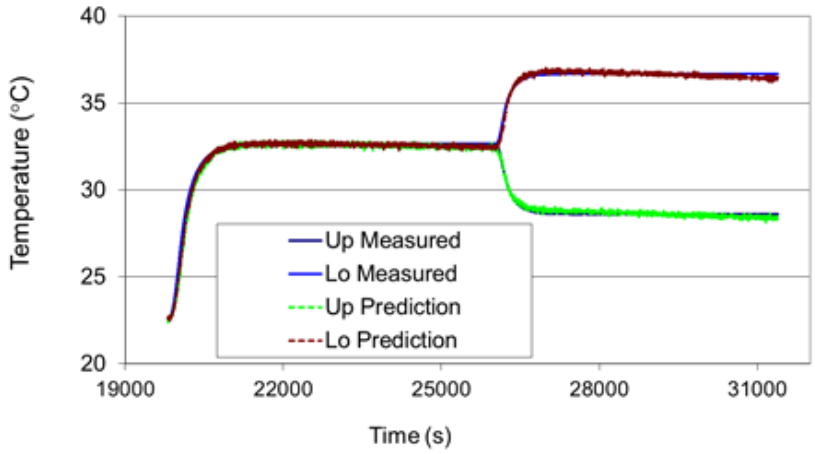

Fig. 4. Interface temperature predictions versus measurement with calibrated thermopile for the extruded PS board (Up = upper copper plate, Lo = lower copper plate)

CONCLUSION

Exact analytical solution to the Luikov's equations for one-dimensional flow in a porous hydroscopic orthotropic material is presented in the time discretization form. The solution is given for three types of stepping boundary conditions: (1) stepping functions of surface temperature and moisture and their surface gradients on just one side of the material, (2) stepping functions of surface temperature and moisture on both sides of the material, and (3) stepping functions of the surface gradients of temperature and moisture on both sides of the material. The recursive solution procedure is implemented in the Excel spreadsheet with Visual Basic Application (VBA) macros. We demonstrated its use in a spreadsheet to fit the data, and by implication it can be used in a computer code as an alternative to finite difference methods.

Because the K-tester was recently refurbished and calibrated to the NIST standard at the factory, one can expect three significant digit accuracy of the thermal conductivity for an ideal steady state condition that includes a uniform material of optimum thickness. This may

suggest a corresponding three significant digits accuracy for the heat capacity considering the high correlation fits to pure and foam PS reference boards. However, independent DSC measurement of the Rexolite fragments can only confirm the heat capacity values to within two significant digits. Therefore, the expectation is for two to three significant digits accuracy for our measurement of simultaneous heat capacity and thermal conductivity for any other specimen, after we have resolved any remaining issues, such as sensitivity to time steps. Indications are that using the larger time steps may make the determination of heat capacity not as accurate, which may be resolved by an alternate implementation or a more sensitive instrument. In any case it is interesting that the same calibration constants to the thermopile are applicable to three PS boards of widely differing density and construction (Rexolite, expanded PS, and extruded PS), which basically provides confirmation of the formulae for heat capacity and thermal conductivity provided. Despite progress made, the quasi-impulse transient method still needs a full evaluation before being a suitable general method for determining thermal properties of wood-based materials. If a material has some nonuniformity, then post-testing can involve cutting the specimen to obtain local density and moisture values needed for their empirical formulation.

ACKNOWLEDGMENTS

We thank Robert Munson for upgrading the Lasercomp K-tester 637 and obtaining the data, and the former researchers Robert White, Ph.D., and Anton TenWolde, Ph.D., and project leader Carol Clausen for their support of this work.

REFERENCES

1. G.J. Kluitenberg, J.M. Ham, and K.L. Bristow, *Soil Sci. Soc. Am. J.*, 57 (1993) 1444-1451.
2. A.J. Nanassy, *Wood Science*, 11(2) (1978) 111-117.
3. W. Yang, S. Sokhansanj, J. Tang, and P. Winter, *Biosystems Engineering* 82, Pt. 2 (2002) 169-176.
4. R.S. Graves, D.W. Yarbrough, D.L. McElroy, and H.A. Fine, *Insulation Materials: Testing and Applications, 2nd Volume*, ASTM STP 1116, Graves and Wysocki, (Eds.), American Society for Testing and Materials, Philadelphia, 1991.
5. W.J. Parker, *Prediction of the Heat Release Rate of Wood*, Ph.D. Dissertation, School of Engineering & Applied Science, George Washington University, Washington, D.C., 1988.
6. A.V. Luikov, *Heat and Mass Transfer in Capillary-Porous Bodies*, Pergamon Press, Oxford, 1966, Chapter 7.
7. J. Y. Liu, *Journal of Heat Transfer*, 113 (1991) 757-762.
8. R.C. Gaur and N.K. Bansal, *Int. J. of Energy Res.*, 23 (1999) 875-885.
9. D. Song, Z-S Liu, and G. Wang, *Numerical Heat Transfer, Part A*, 42 (2002) 585-602.
10. H.S. Carslaw and J.C. Jaeger, *Conduction of Heat in Solids*, 2nd edition reprint, Oxford University Press, 1960, Chapters 1 and 3.
11. L. Zhou, V.M. Puri, R.C. Anantheswaran, *Drying Technology*, 12(3) (1994) 607-627.
12. M.A. Dietenberger, *Journal of thermal analysis and Calorimetry*, Vol. 83 (2006): pages 97-106.
13. R.R. Zarr, M.W. Davis, and F.H. Anderson, "Room-temperature thermal conductivity of expanded polystyrene board for a Standard Reference Material", NISTIR 5838, May, 1996.
14. V. Eveloy, P. Rodgers, and J. Lohan, Proc. 3rd Int. Conf. on Thermal and Mechanical Simulation in Microelectronics, Paris, France, April 14-16 2002.
15. E. Placido, M.C. Arduini-Schuster, and J.Kuhn, *Infared Physics & Technology* vol. 46, 2005, pp. 219-231.

NATAS North American Thermal Analysis Society

September 14-17, 2014
Santa Fe, New Mexico

Technical Program of the 42nd NORTH AMERICAN THERMAL ANALYSIS SOCIETY CONFERENCE